



## Hydrothermal synthesis of Titania nanowires and their photocatalytic activities for Naphthalene

Abubakar Hamisu<sup>1,2\*</sup>, I. Alhassan Auwal<sup>3</sup>

<sup>1</sup>Department of Chemistry, Kano University of Science and Technology  
Wudil, 3244 Kano, Nigeria.

<sup>2</sup>Department of Chemistry, Faculty of Science, Universiti Putra Malaysia,  
43400 UPM Serdang D.E., Malaysia

<sup>3</sup>Chemistry department, Faculty of Natural and applied sciences, Sule Lamido University, PMB 048, Kafin Hausa, Jigawa  
State-Nigeria

Received 19 Nov 2019,  
Revised 21 Jan 2020,  
Accepted 25 Jan 2020

### Keywords

- ✓ Hydrothermal synthesis,
- ✓ TiO<sub>2</sub> nanowires,
- ✓ Calcination temperature,
- ✓ Photocatalysis,
- ✓ Naphthalene.

[ababakary@gmail.com](mailto:ababakary@gmail.com)

Phone: +2348039352016;

Fax: +2348039352016

### Abstract

Hydrothermal synthesis of titanium dioxide nanowires (TNWs) with the reaction of titanium dioxide nanoparticles (Degussa P25) and NaOH aqueous solution was reported in this paper. The synthesized TNWs have been characterized by scanning electron microscopy (SEM), Transmission electron microscopy (TEM), Energy dispersive X-ray (EDX), X-ray diffraction (XRD), and ultraviolet-visible (UV-vis) spectroscopy. The results showed that the synthesized TNW is amorphous material which crystallized after calcination at 500 °C. Red shift in band gap energy was observed when TNW was calcined at 500 °C. The photocatalytic activities of the synthesized TNWs were evaluated by measuring the photocatalytic degradation of naphthalene under UV light irradiation. Effect of calcination temperature on the catalytic performance of the synthesized TNWs was studied. The results reveal that, the increase in the calcination temperature from 100 to 500 °C steadily increases the photocatalytic degradation efficiency of naphthalene and declined at calcination temperature above 500 °C. 500TNW was found to have the highest photocatalytic performance (98.2%).

### 1. Introduction

Nanostructured materials with controlled shapes and structures have attracted substantial attention for both research and practical applications [1-3]. In particular, one dimensional nanostructures such as nanorods, nanowires, and nanotubes are of great importance due to their unique properties and anisotropic structures [4, 5]. One dimensional nanostructures of a wide variety of materials have been successfully synthesized, including carbons (e.g., nanofibers [6] and carbon nanotubes [7]), metalloids (e.g., Ag [8] and Si [9]), and metal oxides (e.g., ZnO [10] and MoO<sub>3</sub> [11]). Much effort has focused on the important metal oxides such as ZnO, TiO<sub>2</sub>, VO<sub>2</sub> and SnO<sub>2</sub> [12]. Titania is a very well-known and well researched material due to its Long-term photostability, inertness to chemical environment, nontoxicity, relatively low cost, strong oxidizing ability, high optical properties, high specific surface area, and high photocatalytic degradation performance under longer wavelength [13-15]. Its photocatalytic properties have been utilized in various environmental applications to remove contaminants from both water and air [12]

As one of the most important metal oxides and semiconductors, Titania has found its applications in a wide range of fields including photocatalysis, solar cells, and lithium-ion batteries [16, 17]. There is a general consensus that the geometric shape and surface property have tremendous effects on the physicochemical properties of TiO<sub>2</sub> [18-20]. TiO<sub>2</sub> nanowires, nanorods, and nanobelts with enhanced performance in photocatalysis, dye-sensitized solar cells, and lithium-ion batteries have been widely reported [5, 21]. For the past few years, many methods have been successfully developed for the fabrication of this nanostructured TiO<sub>2</sub>, including solution-liquid-solid [22], laser ablation [23], arc discharge [24], template-based and synthetic approaches [25]. In most cases, these methods require either a catalyst or templating agents which often contaminate the final product [21]. Hence, it will be interesting to explore a new and facile approach to synthesize TiO<sub>2</sub> that will solve the said draws back. So many synthesis methods for the preparation of nanostructured TiO<sub>2</sub> have been reported such as solvothermal method [26], hydrothermal method [21, 27], sol-gel method [28], chemical vapor deposition [29], direct oxidation method [30], microwave method [31] and electrode deposition [32]. As many different methods and techniques have been developed for the preparation of TiO<sub>2</sub> nanostructured materials, a hydrothermal method for synthesis of titania nanotubes, first proposed by Kasuga et al. [33], has been reported to be the most powerful technique owing to its simplicity, cost-effective and environmentally safe route [34]. Moreover, this technique can also be applied to prepare a wide range of one dimensional titania nanostructures, such as nanowires, and nanoribbons [34, 35]. The hydrothermal treatment at a slightly higher temperature (150 °C or higher) or in stronger alkali solution leads to the formation of solid nanowires or long nanofibers rather than scrolled nanotubes. Although the nanotube structure is attractive due to its high specific surface area, TiO<sub>2</sub> nanotubes are usually unstable at high temperatures and convert into anatase particles [36, 37]. To maintain the one dimensional nanostructure at high temperature, the solid nanowires form should be more favorable [36]. In this work, hydrothermal synthesis of TiO<sub>2</sub> nanowires (TNWs) using Degussa P25 as precursor (commercial TiO<sub>2</sub> powder) was reported. The synthesized TNWs were characterized and applied as photocatalyst. The photocatalytic activities of the synthesized TNWs were evaluated in terms of photocatalytic degradation of naphthalene in water under UV light irradiation. The Effect of calcination temperature on the catalytic performance of the synthesized TNWs was studied.

## **2. Material and Methods**

### *2.1. Material*

Commercial TiO<sub>2</sub> nanoparticle ((P25, 80% anatase and 20% rutile) was used as raw material and purchased from Sigma-Aldrich. Naphthalene (99%) was obtained from MERCK, sodium hydroxide (NaOH, 98%), hydrochloric acid (HCl, fuming 37%) were purchased from R & M Chemical.

### *2.2. Method*

TiO<sub>2</sub> nanowires were prepared through the hydrothermal treatment process using NaOH. In the typical procedure, 1.2 g of the TiO<sub>2</sub> was added into a beaker containing 20 mL of deionized water. The mixture was magnetically stirred for 30 min and sonicated for another 30 min. Then, 20 mL of NaOH (10 M) was added dropwise into the mixture under vigorous stirring and then sonicated for 45 min. Afterward, the mixture was transferred into a 100 mL stainless-steel Teflon-lined autoclave. The autoclave was sealed and placed in an oven at 170°C for 12 h. After the autoclave was naturally cooled to room temperature, the as-synthesized white precipitates were filtered and washed several times with 0.1 M HCl and deionized water to neutral pH level and then oven-dried at 75 °C overnight. Finally, the dried precipitates were calcined at 100 °C, 200 °C, 300 °C, 400 °C, 500 °C, 600 °C and 700 °C for 4 h. For easy identifications, the calcined samples are labelled 100TNW, 200TNW, 300TNW, 400TNW, 500TNW, 600TNW and 700TNW respectively. Moreover, 0TNW denotes the sample without calcination.

### 2.3. Characterization

The morphologies of the samples were analyzed using Transmission electron microscopy (TEM, JEM-2100F FIELD EMISSION ELECTRON MICROSCOPE) and field emission scanning electron microscope (FE-SEM, NOVA NANOSEM 230). Energy dispersive X-ray (EDX) spectra were also obtained from the FE-SEM (NOVA NANOSEM 230). The X-ray diffraction (XRD) patterns of the synthesized TiO<sub>2</sub> nonowires were determined by (Shimadzu XRD-6000 X-RAY DIFFRACTOMETER) employing Cu K $\alpha$  radiation with a wavelength of 0.15406 nm in the range of 20-80° (2 $\theta$ ). The ultraviolet-visible (UV-vis) spectra for determination of band gap were recorded using a UV-Vis spectrophotometer (Shimadzu UV-3600 UV-VIS-NIR SPECTROPHOTOMETER) employing BaSO<sub>4</sub> as the reference in the range of 220-800 nm.

### 2.4. Photocatalytic experiments

The photocatalytic performance of the synthesized photocatalysts was evaluated in relative terms by monitoring the percentage degradation of naphthalene. Experiments were carried out in a previously described photoreactor [38]. The photoreactor was fitted with a new 3 W E14 GMY UV lamp (UV intensity = 450 $\mu$ w/cm<sup>2</sup>, wavelength = 253 nm). In a typical photocatalytic experiment, a solution containing the desired amount of naphthalene and catalyst was added to the photoreactor. Prior to illumination, the mixture was stirred for 30 min in the dark until reaching the adsorption-desorption equilibrium. During the reaction process, oxygen was continuously bubbled through the mixture to avoid change in the concentration of dissolved oxygen. Test samples were taken at periodic intervals of time and filtered using cellulose nitrate membrane (0.45  $\mu$ m). The residual concentration of naphthalene solution was monitored using a UV-Vis spectrophotometer (Perkin Elmer Lambda 35 UV-Vis spectrophotometer) at a wavelength of 272 nm. Percentage degradation of the initial naphthalene concentration was calculated using Eq.(1)

$$D\% = \frac{[\text{Naphthalene}]_0 - [\text{Naphthalene}]_t}{[\text{Naphthalene}]_0} \quad (1)$$

Where [Naphthalene]<sub>0</sub> is the initial Naphthalene concentration, [Naphthalene]<sub>t</sub> is the concentration of Naphthalene at irradiation time *t*. In order to determine kinetic parameters, experiments were performed at optimum conditions for 120 min. Kinetic profiles were plotted according to pseudo-first-order integrated rate equations.

## 3. Results and discussion

### 3.1 Sample morphology and composition

In order to depict the morphology of the obtained TNWs, field emission scanning electron microscopy (FE-SEM) measurements were conducted, with the results shown in Figure 1. It can be seen from Figure 1a that the precursor (P25) shows only the aggregates of titania crystals. After the hydrothermal treatment, the as synthesized or uncalcined (0TNW) shows wire-like morphology with the assembled structure of the nanowires (Figure 1b). Figure 1c depicts the SEM image of 500TNW (calcined at 500 °C) which also shows the assembled structure of nanowires and the size of the nanowires was observed to decreased as compared to 0TNW (Figure 1b). This indicates that post-heat-treatment can decrease the size of the nanowires. However, some nanowires look thicker than others this is because nanowires may aggregate and form. A similar observation was reported by Zhang et al. [21] and Jaturong et al. [36].

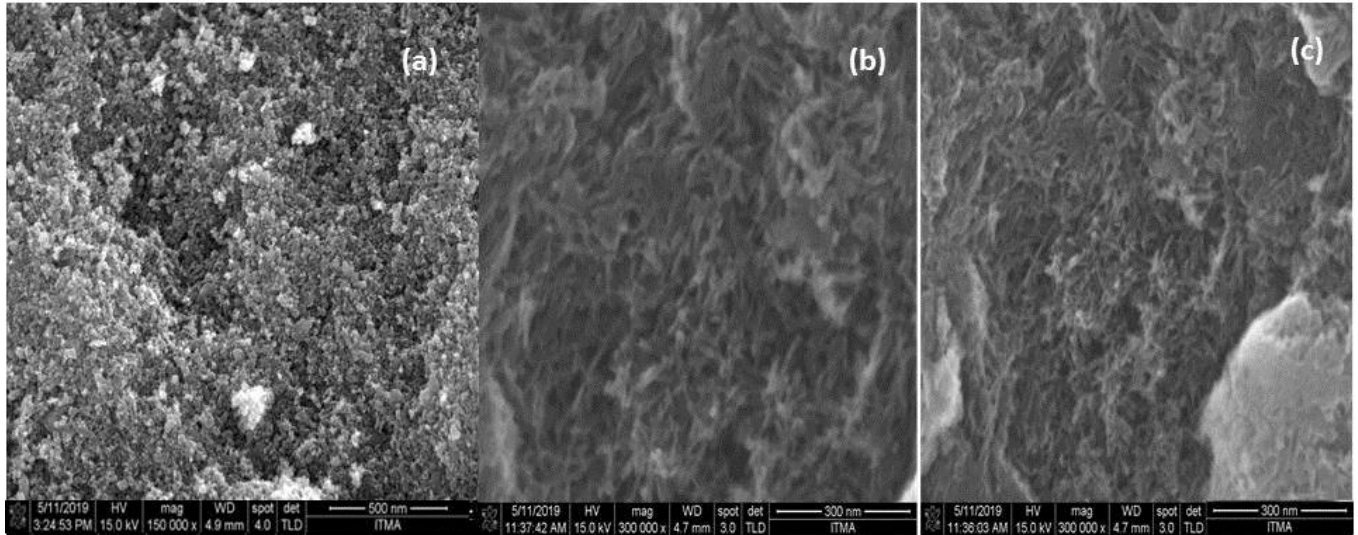


**Figure 1.** The FE-SEM image of (a) P25 (b) 0TNW and (c) 500TNW.

TEM was used to study the fine structure of the nanowires. Figure 2 depicted a typical TEM image of the TiO<sub>2</sub> nanowires (500TNW). From TEM images, one can observe the distinctive solid structure of TNWs, no other morphology (such as hollow structure etc.) was observed. The nano-wires have a diameter of 60-75 nm, and a typical length in the range of 1.5 μ to 2 μ. The assembled structure of nanowires (bundles) was also observed which is in consistent with SEM results.

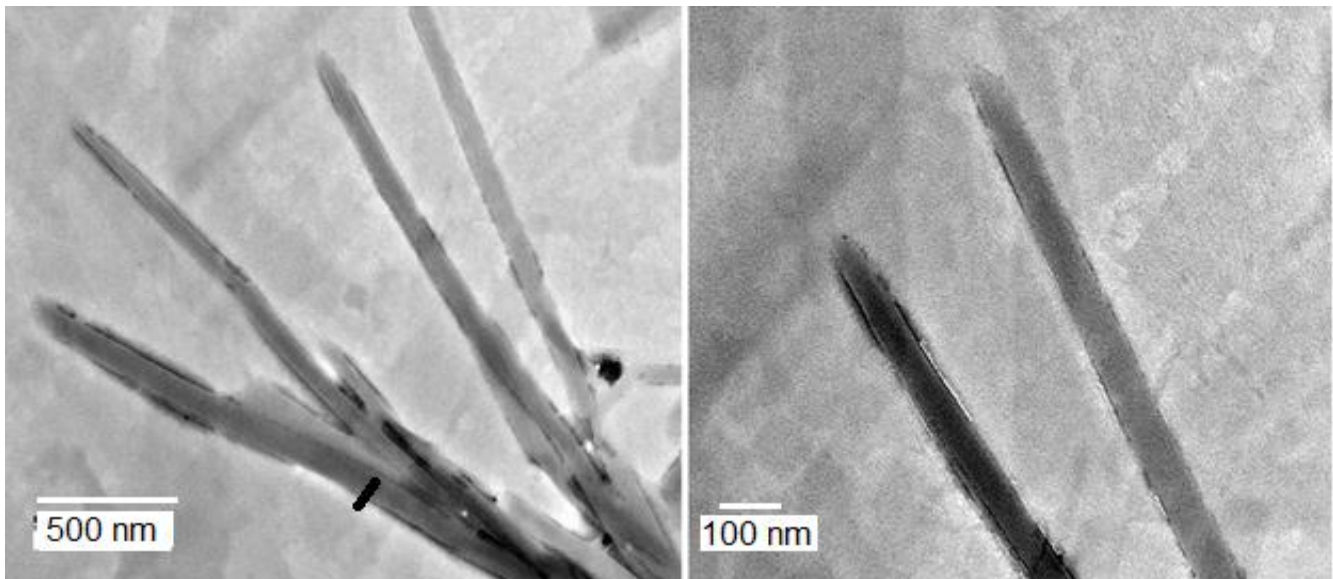


**Figure 2.** The TEM images of 500TNW with different magnification.

The elemental analysis of the sample was carried out by acquiring its EDX spectra. Figure 3 present EDX spectra of 500TNW. The EDX spectra of the sample show peaks correspond to Ti and O which confirmed the TNW is made of TiO<sub>2</sub>.

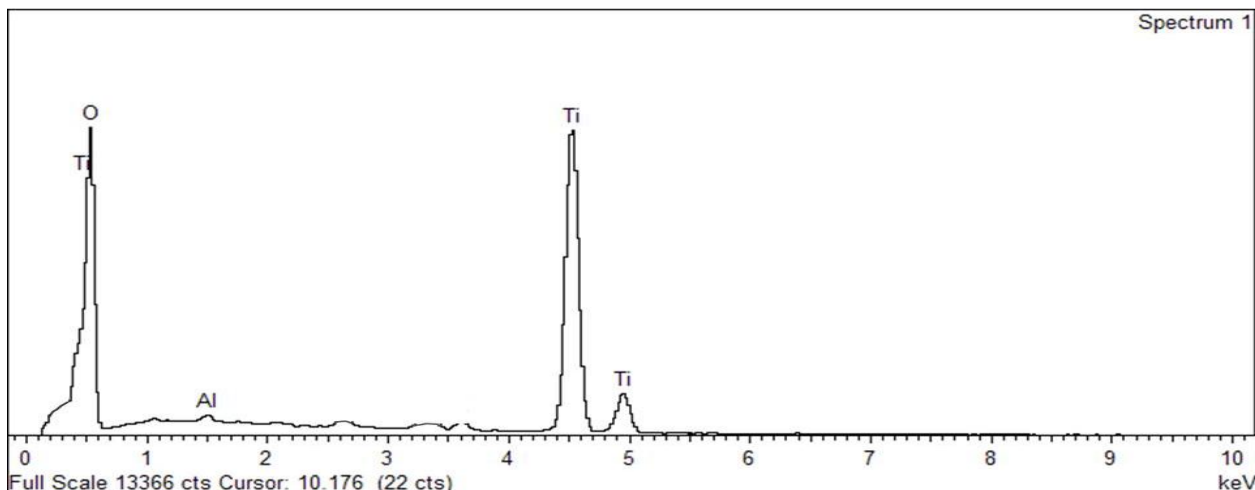


Figure 3. The EDX analysis of 500TNW.

### 3.2 XRD analysis

In order to study the crystalline structures and phase compositions of the samples, X-ray diffraction patterns were collected (Figure 4). The XRD peaks of the samples were studied by comparison with anatase JCPDS-21-1272 [46] and rutile JCPDS-21-1276 [47]. It can be seen from the spectrum, 0TNW (non-calcined sample) shows an amorphous structure in which no defined peak was observed. As several studies showed that most the synthesized TNWs are amorphous which can be converted to anatase or a mixture of anatase and rutile by annealing at high temperature [36, 39, 40]. It can be observed that 500TNW (after calcination at 500 °C) crystalline as displayed in the XRD pattern, which show anatase peaks at  $2\theta$  (and planes) = 25.22(101), 37.73° (004), 47.95° (200), 54.89° (105), 62.83° (204) and rutile peak at  $2\theta$  (and planes) = 27.38° (110).

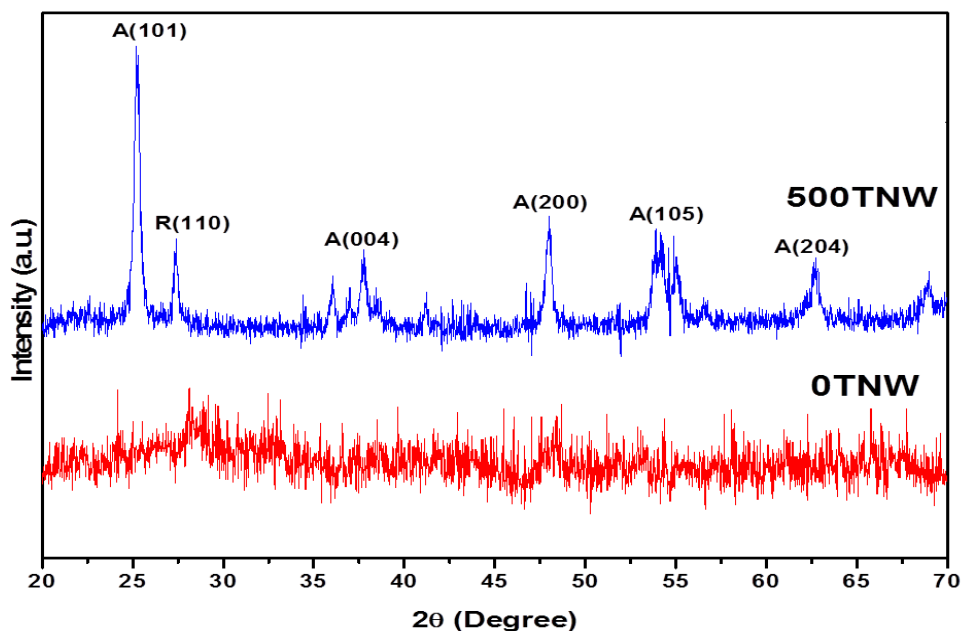
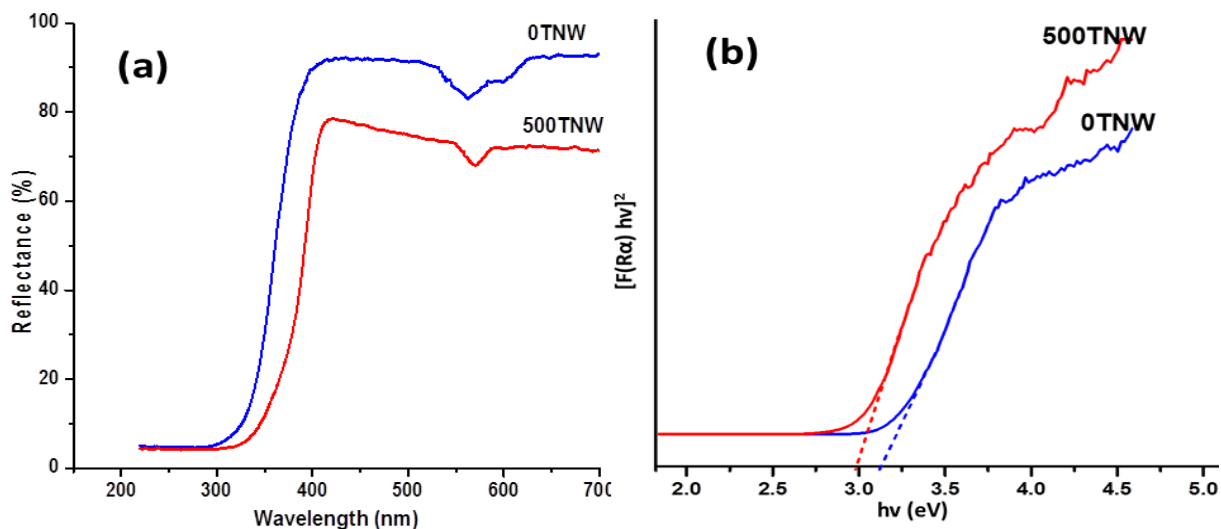


Figure 4. XRD patterns of the samples

### 3.4. Band gap analysis

In order to estimate the band gap energy of the synthesized TNWs, reflectance measurements were carried out over wavelengths of 220–800 nm. The UV–Vis reflectance spectra are displayed in Figure 5a while the band gap energies of the photocatalysts, estimated using the direct method (plot of  $[F(R\alpha)hv]^2$  vs  $hv$ ) [41] are displayed in Figure 5b. The band-gap energy was calculated to be 3.13 and 2.99 eV for 0TNW and 500TNW respectively.



**Figure 5.** (a) UV–vis reflectance spectra of the samples (b) Plot of  $(F(R\alpha)hv)^2$  versus  $hv$  of the samples for band gap evaluation

The results revealed that calcination of the as-synthesized TNW can lead to red shift (narrow band gap energy), and this is could be due to the crystallization of the TNW after calcination. It was strongly believed that the decreased band-gap energy correspond to more power redox abilities for the production of photo-generated electron-hole pairs and strongly reduce the recombination effect, which may contribute to increasing in the photocatalytic performance of materials [42].

### 3.5. Photocatalytic performance of the synthesized TNWs

Photocatalytic degradation of naphthalene was conducted at room temperature in order to investigate the photocatalytic activities of the synthesized materials. To obtain relevant information about the photocatalytic performance, it is necessary to perform experiments from which any possible direct photolysis or adsorption of material on the photocatalyst was excluded. In this regard, experiments were made (i) under UV irradiation without  $TiO_2$  photocatalyst (photolysis) and (ii) in dark with  $TiO_2$  photocatalyst (adsorption). The results showed that in both cases, no significant disappearance of naphthalene was observed ( $< 5\%$  in both cases). The naphthalene removal observed comes predominantly from photocatalytic degradation by TNWs photocatalyst, indicating that the system is working in a pure photocatalytic regime.

Many studies have revealed that calcination is an effective treatment method for improving the photoactivity of nano-structured  $TiO_2$  photocatalysts [43–45, 48]. Figure 6 shows the dependence of % degradation of naphthalene on the calcination temperature. It can be seen from the figure, the increase in the calcination temperature from 100 to 500 °C steadily increases the photocatalytic degradation efficiency of naphthalene. A decline in the degradation efficiency was observed at calcination temperature above 500 °C. Hence, 500 °C is the optimal calcination temperature used in this study. The degradation efficiencies are summarized in Table 1.

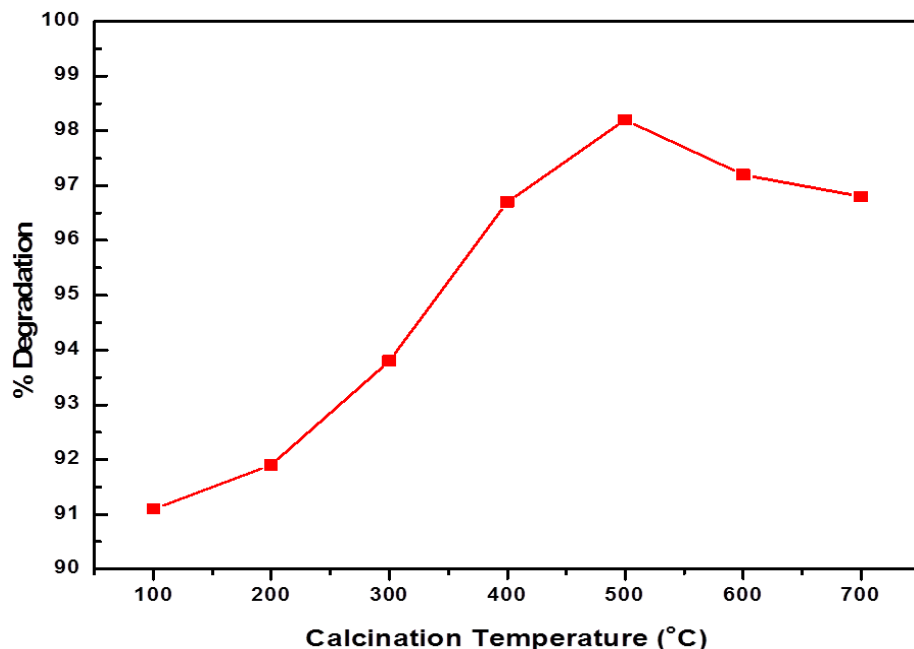


**Figure 6.** Effect of calcination temperature on the performance of the synthesized TNW catalyst (0.8g/L) for degradation of naphthalene (25 ppm) under UV irradiation for 120 min.

The enhancement of photocatalytic performance at elevated temperatures can be attributed to an obvious improvement in the crystallinity of anatase (as shown in Figure 4). At a calcination temperature of 500 °C (500TNW), the highest % degradation of naphthalene (98.2 %) was observed which is higher than P25 and 0TNW as depicted in Figure 7.

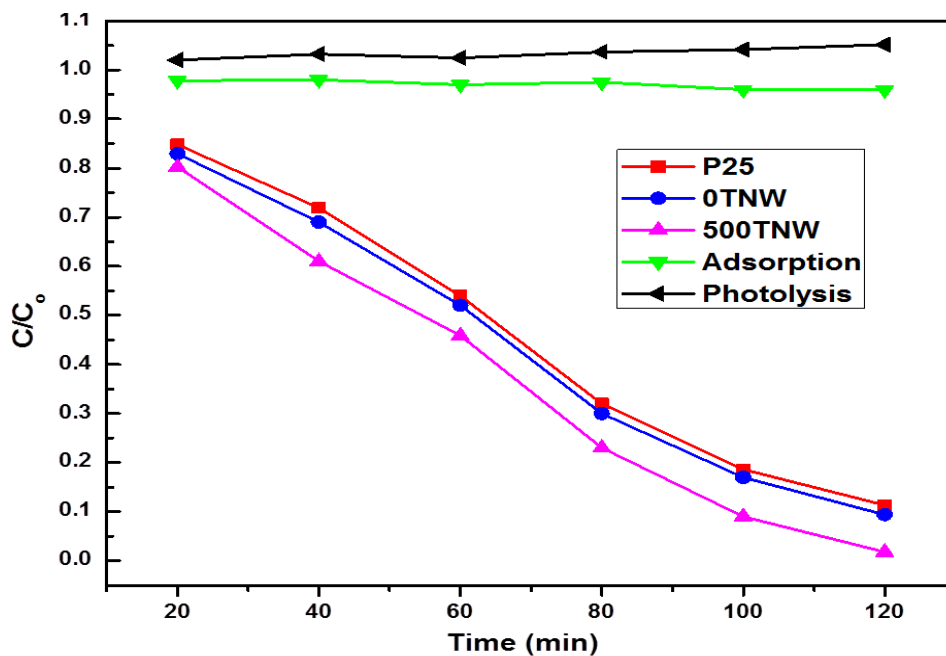


**Figure 7.** Photocatalytic degradation of naphthalene solution (25 ppm) by the synthesized photocatalysts (0.8g/L) under UV irradiation for 120 min.

The high photocatalytic activity of the 500TNW °C can be due to crystallization (Figure 4) and red shift in the band gap energy (Figure 5) of the sample. However, calcination temperatures above 500 °C are not desirable. Sample calcined at 600 and 700 °C display low photocatalytic activity as compared to the sample calcined at 500 °C. Treatment at such a high temperature would form TiO<sub>2</sub> catalysts that are composed of mostly the rutile phase [43].

**Table 1.** Summary of naphthalene photocatalytic degradation under UV irradiation for 120 min

Sample	Calcination Temperature (°C)	% Degradation of naphthalene
P25	-	88.7
0TNW	0	90.6
100TNW	100	91.1
200TNW	200	91.9
300TNW	300	93.8
400TNW	400	96.7
500TNW	500	98.2
600TNW	600	97.2
700TNW	700	96.8

### 3.5. 1. Photocatalytic kinetics

The degradation of naphthalene carried out in this study (Figure 7) can be well fitted by pseudo-first-order kinetics (suggesting that a pseudo-first-order reaction model can be taken into consideration for describing the kinetic behavior). The pseudo-first-order kinetics can be represented by Eq. (2).

$$\ln\left(\frac{[Naphthalene]_0}{[Naphthalene]_t}\right) = kt \quad (2)$$

Where  $[Naphthalene]_0$  and  $[Naphthalene]_t$  indicates the initial concentration of naphthalene and the concentration after a given time  $t$ , while  $k$  is the apparent reaction rate constant (expressed as  $\text{min}^{-1}$ ). A plot of  $\ln([Naphthalene]_0/[Naphthalene]_t)$  versus  $t$  gave a straight line with slope =  $k$  and R square values > 0.8 (Figure 8).

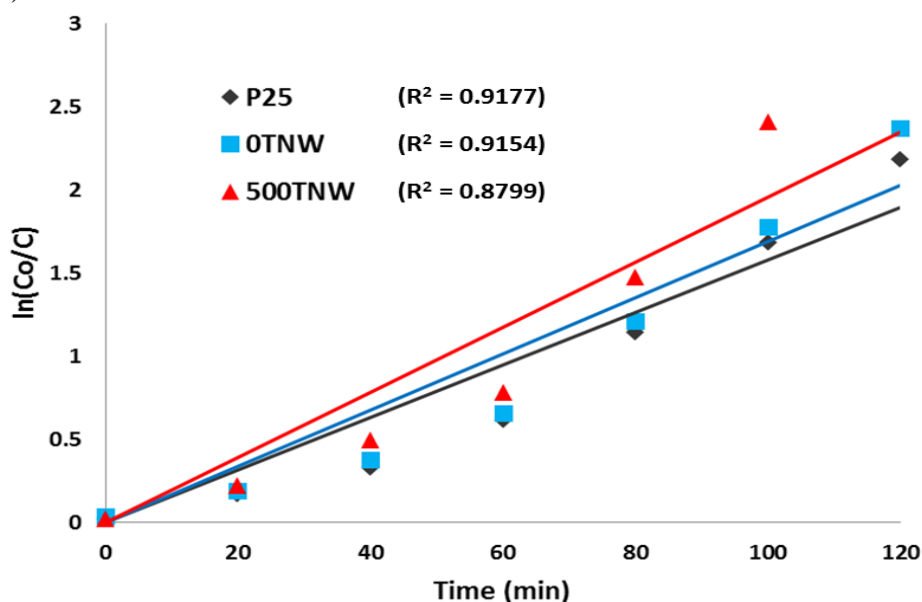


**Figure 8.** Pseudo-first-order graph of naphthalene degradation

## Conclusion

TNW was synthesized via a hydrothermal technique using P25 as a precursor. The TNWs were characterized using different techniques. The XRD results showed that the synthesized TNW is amorphous material which crystallized after calcination at 500 °C. Red shift in band gap energy was observed when TNW was calcined at 500 °C. The photocatalytic activity of the synthesized TNWs was studied by photocatalytic degradation of naphthalene. The increase in the calcination temperature from 100 to 500 °C steadily increases the photocatalytic degradation efficiency of naphthalene. A decline in the degradation efficiency was observed at calcination temperature above 500 °C. 500TNW was found to have the highest photocatalytic performance (98.2%), which may be due to crystallization and red shift in band gap energy of the sample.

## References

1. X. Wang, J. Zhuang, Q. Peng, Y. Li, A general strategy for nanocrystal synthesis, *Nature*, 437 (2005) 121-124. <https://www.nature.com/articles/nature03968>
2. Y. Xia, Y. Xiong, B. Lim, S.E. Skrabalak, Shape-controlled synthesis of metal nanocrystals: simple chemistry meets complex physics?, *Angew. Chem. Int. Ed.* 48 (2009) 60-103. <https://doi.org/10.1002/anie.2008022488>
3. Y. Yin, A.P. Alivisatos, Colloidal nanocrystal synthesis and the organic-inorganic interface, *Nature* 437 (2005) 664-670. <https://doi.org/10.1038/nature04165>
4. M. Law, L.E. Greene, J.C. Johnson, R. Saykally, P. Yang, Nanowire dye-sensitized solar cells, *Nat. Mater.* 4 (2005) 455-459. <https://doi.org/10.1038/nmat1387>
5. H. B. Wu, H.H. Hng, X.W. Lou, Direct synthesis of anatase TiO<sub>2</sub> nanowires with enhanced photocatalytic activity, *Adv Mater.* 24 (2012) 2567-2571. <https://doi.org/10.1002/adma.201200564>
6. E. Hammel, X. Tang, M. Trampert, T. Schmitt, K. Mauthner, A. Eder, P. Pötschke, Carbon nanofibers for composite applications, *Carbon.* 42 (2004) 1153-1158. <https://doi.org/10.1016/j>
7. S. Iijima, Helical microtubules of graphitic carbon, *Nature.* 354 (1991) 56-58. <https://doi.org/10.1038/354056a0>
8. B. H. Hong, S.C. Bae, C.W. Lee, S. Jeong, K.S. Kim, Ultrathin single-crystalline silver nanowire arrays formed in an ambient solution phase, *Science.* 294 (2001) 348-351. <https://doi.org/10.1126/science.1062126>
9. J. D. Holmes, K.P. Johnston, R.C. Doty, B.A. Korgel, Control of thickness and orientation of solution-grown silicon nanowires, *Science.* 287 (2000) 1471-1473. <https://doi.org/10.1126/science.287.5457.1471>
10. P. Yang, H. Yan, S. Mao, R. Russo, J. Johnson, R. Saykally, N. Morris, J. Pham, R. He, H.J. Choi, Controlled growth of ZnO nanowires and their optical properties, *Adv. Funct. Mater.* 12 (2002) 323-331. [https://doi.org/10.1002/1616-3028\(20020517\)12:5<323::AID-ADFM323>3.0.CO;2-G](https://doi.org/10.1002/1616-3028(20020517)12:5<323::AID-ADFM323>3.0.CO;2-G)
11. X.W. Lou, H.C. Zeng, Hydrothermal synthesis of  $\alpha$ -MoO<sub>3</sub> nanorods via acidification of ammonium heptamolybdate tetrahydrate, *Chem Mater.* 14 (2002) 4781-4789. <https://doi.org/10.1021/acs.jpcc.7b11295>
12. M. Malekshahi Byranvand, A. Nematı Kharat, L. Fatholahi, Z. Malekshahi Beiranvand, A review on synthesis of nano-TiO<sub>2</sub> via different methods, *J. Nanostruct.* 3 (2013) 1-9. <https://doi:10.7508/JNS.2013.01.001>
13. M. Zulfiqar, A.A. Omar, S. Chowdhury, Synthesis and characterization of single-layer TiO<sub>2</sub> nanotubes, *Adv Mat Res. Trans Tech Publ* (2016) 501-504. <https://doi.org/10.4028/www.scientific.net/AMR.1133.501>
14. W.T. Chang, Y.C. Hsueh, S.-H. Huang, K.I. Liu, C.C. Kei, T.P. Perng, Fabrication of Ag-loaded multi-walled TiO<sub>2</sub> nanotube arrays and their photocatalytic activity, *J. Mater. Chem A.* 1 (2013) 1987-1991. <https://doi.org/10.1039/C2TA00806H>
15. M. Zulfiqar, S. Chowdhury, A. Omar, Hydrothermal synthesis of multiwalled TiO<sub>2</sub> nanotubes and its photocatalytic activities for Orange II removal, *Sep Sci Technol.* 53 (2018) 1412-1422. <https://doi:10.1080/01496396.2018.1444050>

16. A.O. Ibhaddon, P. Fitzpatrick, Heterogeneous photocatalysis: recent advances and applications, *Catalysts*, 3 (2013) 189-218. <https://doi.org/10.3390/catal3010189>.
17. U.I. Gaya, A.H. Abdullah, Heterogeneous photocatalytic degradation of organic contaminants over titanium dioxide: a review of fundamentals, progress and problems, *J Photoch photobio C*. 9 (2008) 1-12. <https://doi.org/10.1016/j.jphotochemrev.2007.12.003>
18. J. Pan, G. Liu, G.Q. Lu, H.M. Cheng, On the true photoreactivity order of {001}, {010}, and {101} facets of anatase TiO<sub>2</sub> crystals, *Angew Chem Int Ed*. 50 (2011) 2133-2137. <https://DOI:10.1002/anie.201006057>.
19. N. Wu, J. Wang, D.N. Tafen, H. Wang, J. G. Zheng, J.P. Lewis, X. Liu, S.S. Leonard, A. Manivannan, Shape-enhanced photocatalytic activity of single-crystalline anatase TiO<sub>2</sub> (101) nanobelts, *J Am Chem Soc*. 132 (2010) 6679-6685. <https://doi: 10.1021/ja909456f>.
20. Z. Sun, J.H. Kim, Y. Zhao, F. Bijarbooneh, V. Malgras, Y. Lee, Y.-M. Kang, S.X. Dou, Rational design of 3D dendritic TiO<sub>2</sub> nanostructures with favorable architectures, *J Am Chem Soc*. 133 (2011) 19314-19317. <https://doi: 10.1021/ja208468d>.
21. Y. Zhang, G. Li, Y. Jin, Y. Zhang, J. Zhang, L. Zhang, Hydrothermal synthesis and photoluminescence of TiO<sub>2</sub> nanowires, *Chem. Phys. Lett*. 365 (2002) 300-304. [https://DOI: 10.1016/S0009-2614\(02\)01499-9](https://DOI: 10.1016/S0009-2614(02)01499-9).
22. T.J. Trentler, K.M. Hickman, S.C. Goel, A.M. Viano, P.C. Gibbons, W.E. Buhro, Solution-liquid-solid growth of crystalline III-V semiconductors: an analogy to vapor-liquid-solid growth, *Science*. 270 (1995) 1791-1794. <https://DOI: 10.1126/science.270.5243.1791>
23. M. Morales, C.M. Lieber, A laser ablation method for the synthesis of crystalline semiconductor nanowires, *Science*. 279 (1998) 208-211. <https://DOI: 10.1126/science.279.5348.208>
24. Y.C. Choi, W.S. Kim, Y.S. Park, S.M. Lee, D.J. Bae, Y.H. Lee, G.S. Park, W.B. Choi, N.S. Lee, J.M. Kim, Catalytic growth of β-Ga<sub>2</sub>O<sub>3</sub> nanowires by arc discharge, *Adv. Mater*. 12 (2000) 746-750. [https://doi.org/10.1002/\(SICI\)1521-4095\(200005\)12:10<746::AID-ADMA746>3.0.CO;2-N](https://doi.org/10.1002/(SICI)1521-4095(200005)12:10<746::AID-ADMA746>3.0.CO;2-N)
25. C.R. Martin, Nanomaterials: a membrane-based synthetic approach, *Science*. 266 (1994) 1961-1966. <https://DOI: 10.1126/science.266.5193.1961>
26. R.K. Wahi, Y. Liu, J.C. Falkner, V.L. Colvin, Solvothermal synthesis and characterization of anatase TiO<sub>2</sub> nanocrystals with ultrahigh surface area, *J Colloid Interf Sci*. 302 (2006) 530-536. <https://DOI:10.1016/j.jcis.2006.07.003>.
27. J. Yu, L. Zhang, B. Cheng, Y. Su, Hydrothermal preparation and photocatalytic activity of hierarchically sponge-like macro-/mesoporous titania, *J Phys Chem C*. 111 (2007) 10582-10589. <https://doi.org/10.1021/jp0707889>.
28. H. Bazargan, M.M. Byranvand, A.N. Kharat, Preparation and characterization of low temperature sintering nanocrystalline TiO<sub>2</sub> prepared via the sol-gel method using titanium (IV) butoxide applicable to flexible dye sensitized solar cells, *Int. J Mater. Res*. 103 (2012) 347-351. <https://doi:10.3139/146.110644>
29. S. C. Bhosale, Properties of chemical vapour deposited nanocrystalline TiO<sub>2</sub> thin films and their use in dye-sensitized solar cells, *J. Anal Appl. Pyrol*. 82 (2008) 83-88. <https://doi.org/10.1016/j.jaap.2008.01.004>
30. W.H. Ryu, C.J. Park, H.S. Kwon, Synthesis of highly ordered TiO<sub>2</sub> nanotube in malonic acid solution by anodization, *J Nanosci Nanotechno*. 8 (2008) 5467-5470. <https://DOI:10.1166/jnn.2008.1141>
31. A.B. Corradi, F. Bondioli, B. Focher, A.M. Ferrari, C. Grippo, E. Mariani, C. Villa, Conventional and microwave-hydrothermal synthesis of TiO<sub>2</sub> nanopowders, *J Am Ceram Soc*. 88 (2005) 2639-2641. <https://doi:10.3390/ma12071177>
32. W. Tan, J. Chen, X. Zhou, J. Zhang, Y. Lin, X. Li, X. Xiao, Preparation of nanocrystalline TiO<sub>2</sub> thin film at low temperature and its application in dye-sensitized solar cell, *J Solid State Electr*. 13 (2009) 651-656. <https:// DOI: 10.1007/s10008-008-0605-4>
33. T. Kasuga, M. Hiramatsu, A. Hoson, T. Sekino, K. Niihara, Formation of titanium oxide nanotube, *Langmuir*. 14 (1998) 3160-3163. <https://doi.org/10.1021/la9713816>
34. E. Morgado, M.A. de Abreu, G.T. Moure, B.A. Marinkovic, P.M. Jardim, A.S. Araujo, Characterization of nanostructured titanates obtained by alkali treatment of TiO<sub>2</sub>-anatases with distinct crystal sizes, *Chem Mater*. 19 (2007) 665-676. <https://doi.org/10.1021/cm061294b>
35. Z.Y. Yuan, B.L. Su, Titanium oxide nanotubes, nanofibers and nanowires, *Colloid Surface A*. 241 (2004) 173-183. <https://doi.org/10.1016/j.colsurfa.2004.04.030>

36. J. Jitputti, S. Pavasupree, Y. Suzuki, S. Yoshikawa, Synthesis of TiO<sub>2</sub> nanotubes and its photocatalytic activity for H<sub>2</sub> evolution, *Jpn J Appl Phys.* 47 (2008) 751. [https:// DOI: 10.1143/JJAP.47.751](https://doi.org/10.1143/JJAP.47.751)
37. R. Yoshida, Y. Suzuki, S. Yoshikawa, Syntheses of TiO<sub>2</sub> (B) nanowires and TiO<sub>2</sub> anatase nanowires by hydrothermal and post-heat treatments, *J Solid State Chem.* 178 (2005) 2179-2185. <https://doi.org/10.1016/j.jssc.2005.04.025>
38. U.I. Gaya, A.H. Abdullah, Z. Zainal, M.Z. Hussein, Photocatalytic treatment of 4-chlorophenol in aqueous ZnO suspensions: Intermediates, influence of dosage and inorganic anions, *J Hazard Mater.* 168 (2009) 57-63. <https://doi.org/10.1016/j.jhazmat.2009.01.130>
39. P. Roy, S. Berger, P. Schmuki, TiO<sub>2</sub> nanotubes: synthesis and applications, *Angew Chem Int Ed.* 50 (2011) 2904-2939. [https:// doi: 10.1002/anie.201001374.](https://doi.org/10.1002/anie.201001374)
40. M. Macak, H. Tsuchiya, A. Ghicov, K. Yasuda, R. Hahn, S. Bauer, P. Schmuki, TiO<sub>2</sub> nanotubes: Self-organized electrochemical formation, properties and applications, *Curr Opin Solid St M.* 11 (2007) 3-18. <https://DOI: 10.1016/j.cossms.2007.08.004>
41. R. López, R. Gómez, Band-gap energy estimation from diffuse reflectance measurements on sol-gel and commercial TiO<sub>2</sub>: a comparative study, *J Sol-gel Sci Techn.* 61 (2011) 1-7. [https://doi.org/10.1007/s10971-011-2582-9.](https://doi.org/10.1007/s10971-011-2582-9)
42. X. Zhao, P. Wu, M. Liu, D. Lu, J. Ming, C. Li, J. Ding, Q. Yan, P. Fang, Y<sub>2</sub>O<sub>3</sub> modified TiO<sub>2</sub> nanosheets enhanced the photocatalytic removal of 4-chlorophenol and Cr (VI) in sun light, *Appl Surf Sci.* 410 (2017) 134-144. <https://doi.org/10.1016/j.apsusc.2017.03.073>
43. J.C. Yu, J. Yu, W. Ho, Z. Jiang, L. Zhang, Effects of F-doping on the photocatalytic activity and microstructures of nanocrystalline TiO<sub>2</sub> powders, *Chem Mater.* 14 (2002) 3808-3816. <https://doi.org/10.1021/cm020027c>
44. H. Kominami, S.y. Murakami, M. Kohno, Y. Kera, K. Okada, B. Ohtani, Stoichiometric decomposition of water by titanium (IV) oxide photocatalyst synthesized in organic media: Effect of synthesis and irradiation conditions on photocatalytic activity, physical chemistry chemical physics, *Phys Chem Chem Phys.* 3 (2001) 4102-4106. <https://doi.org/10.1039/B103912C>
45. H. Tanaka, M. Sukanuma, Effects of heat treatment on photocatalytic property of sol-gel derived polycrystalline TiO<sub>2</sub>, *J. Sol-Gel Sci. Techn.* 22 (2001) 83-89. <https:// DOI: 10.1023/A:1011268421046>
46. P. Mathumba , A. T. Kuvarega, L. N. Dlamini, S. P. Malinga, Synthesis and characterisation of titanium dioxide nanoparticles prepared within hyperbranched polyethylenimine polymer template using a modified sol-gel method, *Mater. Lett.* 5(2017) 177-172. <https://doi.org/10.1016/j.matlet.2017.02.108>
47. F. Scarpelli, T. F. Mastropietro, T. Poerio, N. Godbert, Mesoporous TiO<sub>2</sub> thin films: State of the art, *Titanium Dioxide: Material for a Sustainable Environment*, 57 (2018), <http://dx.doi.org/10.5772/intechopen.74244>
48. L.A. Al-Hajji, A. A. Ismail, A. Al-Hazza, S.A. Ahmed, M. Alsaidi, F. Almutawa, Impact of calcination of hydrothermally synthesized TiO<sub>2</sub> nanowires on their photocatalytic efficiency, *J. Mol. Struct.* 1200 (2020) 127153. <https://doi.org/10.1016/j.molstruc.2019.127153>

(2020) ; <http://www.jmaterenvironsci.com>